Journal of Power Sources 268 (2014) 645–657

Contents lists available at ScienceDirect

Journal of Power Sources

journal homepage: www.elsevier.com/locate/jpowsour

Surface film formation on TiSnSb electrodes: Impact of electrolyte additives

W. Zhang [a, b], F. Ghamouss [b], A. Darwiche [c], L. Monconduit [c], D. Lemordant [b], R. Dedryvère [a], H. Martinez [a, *]

[a] IPREM-ECP CNRS UMR 5254, Université de Pau, Hélioparc Pau Pyrénées, 2 av. Pierre Angot, 64053 Pau Cedex 9, France
[b] PCM2E, Université F. Rabelais, Parc de Grandmont, 37200 Tours, France
[c] ICG-AIME, Bat 15, cc 15-02 Université Montpellier 2, Pl. E. Bataillon, 34095 Montpellier cedex, France

HIGHLIGHTS

- The addition of VC and FEC as electrolyte additives enhanced electrochemical properties of TiSnSb electrode.
- The SEI layer formed on TiSnSb electrode partially dissolved upon cycling.
- The formation of a thinner and more conductive SEI layer using electrolyte additives is confirmed.
- The composition of the SEI layer is modified by the chosen electrolyte additives.

ARTICLE INFO

Article history:
Received 20 March 2014
Received in revised form
21 May 2014
Accepted 8 June 2014
Available online 25 June 2014

Keywords:
Li-ion batteries
TiSnSb
Solid electrolyte interphase
XPS
EIS
SEM

ABSTRACT

X-ray photoelectron spectroscopy (XPS), scanning electron microscopy (SEM), and electrochemical impedance spectroscopy (EIS) have been performed to study the formation of surface film on TiSnSb, a promising conversion anode material for lithium ion battery. TiSnSb electrodes were cycled using a standard EC/PC/3DMC (1 M $LiPF_6$) electrolyte containing vinylene carbonate (VC) as a primary filming agent. Fluoroethylene carbonate (FEC) was added as an additional additive intended to improve the stability of the surface film and, hence, the cyclability of the electrode. Surface analysis was performed by a combined XPS core peaks and quantification data analysis to establish the main components of the solid electrolyte interphase film (SEI) were identified. The key observation is that the thickness and the chemical nature of the SEI layer is strongly related to the nature of the electrolyte additives. From XPS and EIS results, the role of FEC as an effective SEI improver in alkylcarbonate based electrolyte has been enlighten.

1. Introduction

Rechargeable Li-ion batteries have been widely used for various portable applications due to their high energy densities [1]. As the conventional graphite electrode is limited by its theoretical capacity of 372 mAh g^{-1} [2], further improvement in term of capacity will require new materials. One of the possible ways for that is to focus on Sb [3–7] and Sn-based [8–11] conversion materials which exhibit high storage capacities. The conversion equation involved is given in Eq. (1), where M designs Sn or Sb:

$$M + xLi^{+} + xe^{-} \leftrightarrow Li_xM \quad (1)$$

For instance, the Li rich $Li_{22}Sn_5$ phase is able to theoretically accommodate 22Li for 5Sn which leads to a theoretical capacity of 994 mAh g^{-1}. In the case of Sb, Li_3Sb gives a theoretical capacity of 660 mAh g^{-1} [12]. However, conversion materials suffer from drastic volume change during lithium insertion/extraction. As an example, the lattice of the tin antimony alloy (SnSb) expands to 137% when it accommodates 6.5 lithium. This volume change causes high mechanical strains which results in the loss of mechanical properties and finally to fast capacity fading. This phenomenon has to be overcome prior to the commercialization of batteries using Sb- and Sn-based materials as anodes. With the aim to get around this obstacle many efforts have been done to minimize the size of active particles but this not effectively improve the cyclability of Sn-based materials due to the fact that nano-particles tend to aggregate and form inactive dense blocks after several cycles [13]. Another way to improve the cyclability of the SnSb alloy is

* Corresponding author. Tel.: +33 5 59407599; fax: +33 5 59407622.
E-mail address: herve.martinez@univ-pau.fr (H. Martinez).

http://dx.doi.org/10.1016/j.jpowsour.2014.06.041
0378-7753/

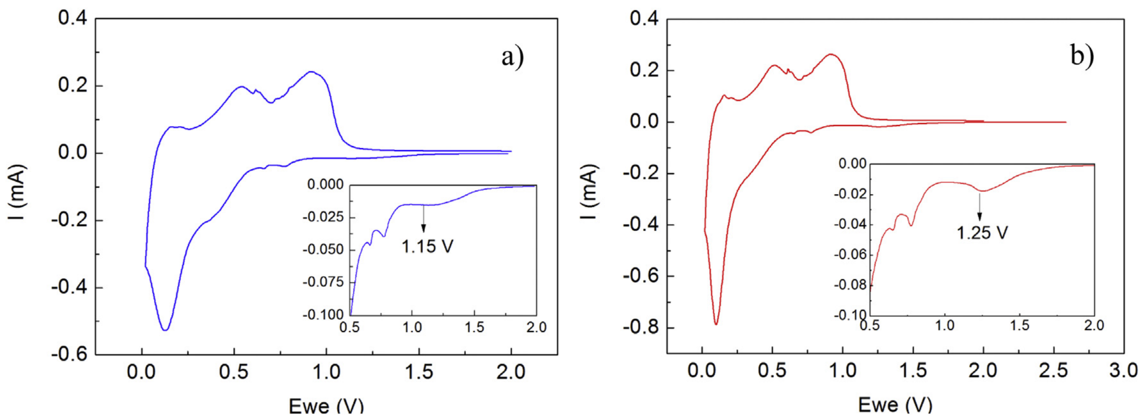

Fig. 1. Cyclic voltammograms of TiSnSb electrode at 0.025 mV s^{-1} between 0.02 and 2.0 V, a) without FEC, b) with FEC.

to introduce transition metal such as titanium in order to create a buffering matrix [14]. In fact, the use of intermetallic or composite active/inactive materials instead of a pure metal seems to be an effective way to control the volume changes [15]. During discharge, Ti remains electrochemically inactive when Sn or Sb reacts with Li, in which way the buffering effect helps to increase the mechanical resistance to the volume expansion, and to retain the initial capacity of the electrode material. With this goal, TiSnSb has been developed as a negative electrode material for Li-ion batteries as this conversion material can reversibly take up 6.5 lithium per formula unit leading to a theoretical capacity of 580 mAh g^{-1} with noteworthy high rate capabilities [16,17]. In the following, the 1 C rate will be defined by the insertion of 1Li in 1 h. The conversion reaction may be summarized by Eq. (2):

$$TiSnSb + 6.5Li \rightarrow Ti + Li_3Sb + 0.5Li_7Sn_2 \quad (2)$$

It is generally admitted that the capacity retention and storage life of Li-ion batteries directly depend on the formation of a passivation film at its surface which is usually known as a solid electrolyte interphase (SEI) [18–22]. The SEI layer originates from the reductive decomposition of the electrolyte at the electrode surface. The role of the SEI is to build up a protective film that not only supports Li$^+$ ions migration during cycling, but also prevents side reactions such as solvent co-intercalation as in graphite and further decomposition of electrolyte components [23]. Since the formation of SEI layer plays a crucial role in the cycling ability of the electrode, it is very important to understand the mechanism which leads to its formation as well as the composition of this layer. The most convenient way to improve the quality of the SEI layer is to use SEI forming additives such as vinyl carbonate (VC). Using $LiCoO_2$/graphite batteries, it has been demonstrated [24] that the radical polymer poly(VC) is the main VC-derived product contributing to the formation of the surface film. VC has also been applied to improve the cycle life of other systems such as Si thin films [25–27], Si-based composite electrodes [28], and Si-nanowire (SiNW) electrodes [29]. Besides VC, FEC has also been proposed as a SEI improver, as it reduces before EC and others alkylcarbonates and contributes to form a more stable SEI. Long chain flexible polycarbonates could be the major surface film component in FEC and VC-containing electrolyte solutions [29]. This polymeric surface film may explain the ability of the electrode to accommodate large volume expansions as it is the case for Si. This SEI film is also able to limit the contact between the electrode material and the liquid electrolyte. FEC also promotes longer cycle life in the case of sodium batteries using Sb anode [30] and hard carbon anode [31]. The addition of FEC and VC favors the precipitation of more stable degradation products limiting further EC decomposition and strongly improving the electrochemical performances [28]. Recently, VC and FEC-containing electrolyte has also been reported to significantly enhance the cycling ability of conversion material like TiSnSb used as a negative electrode in Li-ion batteries [32].

In this study, X-ray photoelectron spectroscopy (XPS) and electrochemical impedance spectroscopy (EIS) were carried out to

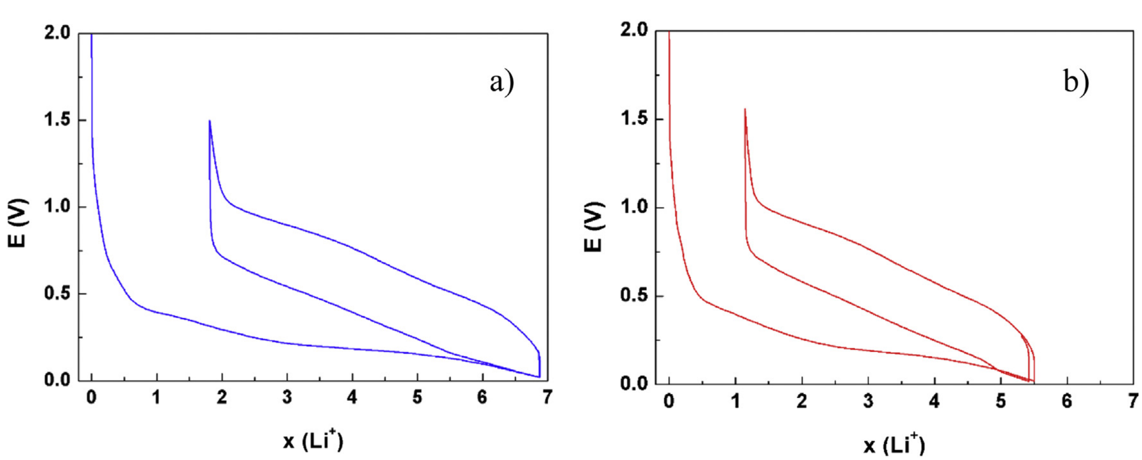

Fig. 2. 1st Galvanostatic discharge/charge galvanostatic curves of a TiSnSb electrode cycled at 4 C rate between 0.02 and 1.5 V, a) without FEC, b) with FEC.

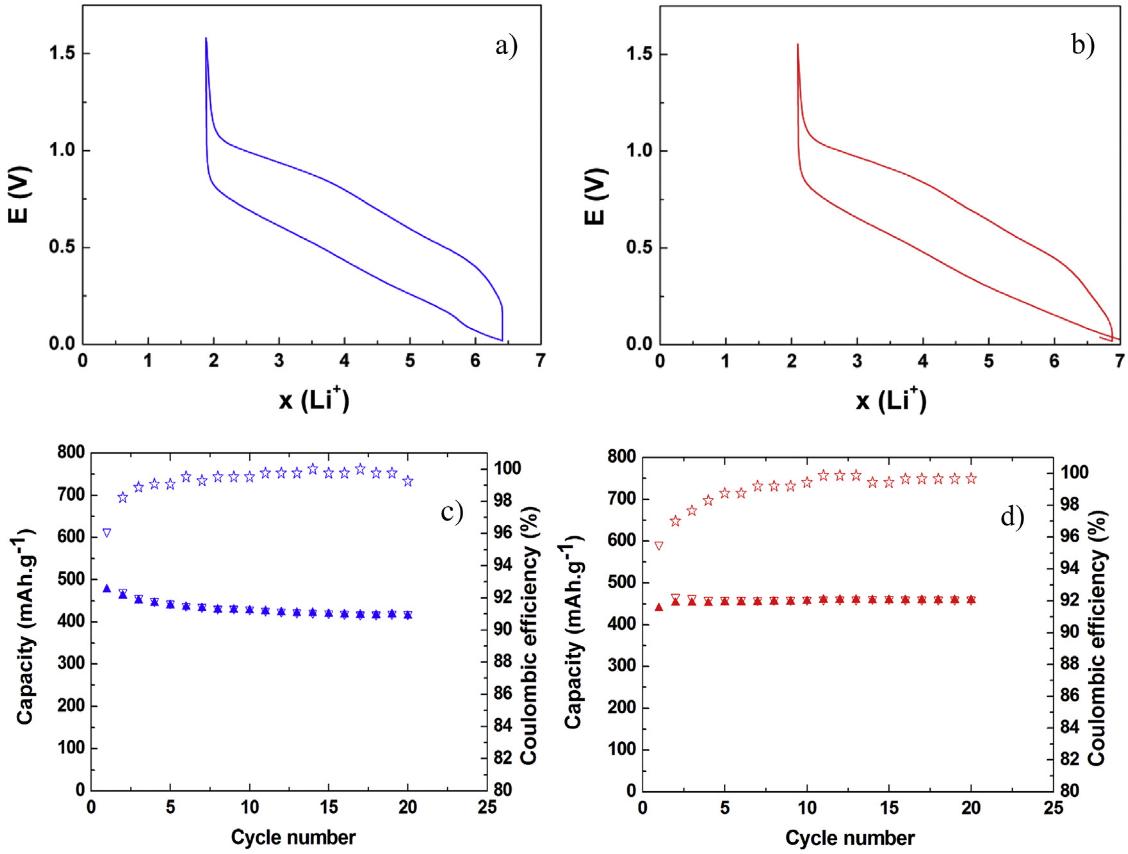

Fig. 3. Galvanostatic curve of a TiSnSb electrode cycled at 4 C rate between 0.02 and 1.5 V in the standard electrolyte at the 20th discharge/charge cycle: a) without FEC, b) with FEC. Capacities curves vs cycle number: c) without FEC, d) with FEC.

carefully investigate the physical properties and chemical composition of the SEI layer formed at the TiSnSb electrode surface in the presence or not of SEI forming additives.

2. Experimental section

2.1. Electrochemical tests

TiSnSb electrodes were prepared by mixing TiSnSb microparticles, carbon conductive additives (vapor grown carbon fibers VGCF, carbon black CB) and CMC-Na binder as described in previous works [16,17,32]. TiSnSb electrodes were cycled against lithium using the EC/PC/3DMC (1 M $LiPF_6$) with VC (1% wt) as the standard electrolyte to which FEC (5% wt) was added as SEI forming improver. Two-electrode Swagelok cells were assembled in a glovebox using the composite electrode as positive electrode, microporous Celgard membrane (Celgard 2400) and WHATMAN glass-fiber paper filled with the electrolyte solution as separator, and metallic lithium as negative electrode. Cells were cycled at 20 °C using a VMP system (Bio-Logic S.A.) in galvanostatic mode from 0.02 to 1.5 V vs Li^+/Li at 4 C rate (i.e. 4Li in 1 h). Cyclic voltammetry was conducted at a scan rate of 25 $\mu V\ s^{-1}$ from the OCV to 20 mV vs Li^+/Li and then to a set potential of 1.6 V vs Li/Li^+.

Three electrodes Swagelok-type cells, with lithium foils as counter and reference electrodes were assembled in an argon-filled glovebox to perform electrochemical impedance spectroscopy (EIS) measurement. Whatman paper filters, filled with the electrolyte solution, were used as separator. EIS data were obtained under the potentiostatic mode in the frequency range from 1 MHz to 2 mHz with an amplitude of 10 mV by using a multichannel galvanostat–potentiostat (VMP-Bio-Logic S.A.) piloted by an EC Lab V10.32 interface. Spectra were presented according to Nyquist representation EIS were recorded at the OCV after assembling the cell and then under cycling at 1 C or 4 C rate at the end of discharge (0.02 V) of each cycle. The impedance of the cell was measured in the potentiostatic mode (PEIS).

Table 1
XPS quantification data recorded at the end of the 1st discharge without FEC (D1-4C), at the end of the 1st charge without FEC (C1-4C), at the end of the 1st discharge with FEC (D1-4C-FEC), and at the end of the 1st charge with FEC (C1-4C-FEC).

	D1-4C		C1-4C		D1-4C-FEC		C1-4C-FEC	
	B.E. (eV)	Atom (%)	B.E. (eV)	Atom (%)	B.E. (eV)	Atom (%)	B.E. (eV)	Atom (%)
C 1s	285.0	(7.7)	285.0	(10.1)	285.0	(16.6)	285.0	(19.9)
	286.6	(0.9)	286.6	(4.2)	286.4	(3.7)	286.4	(13.8)
	289.0	(1.0)	289.0	(2.3)	289.2	(2.1)	288.9	(4.8)
	290.2	(13.4)	290.2	(11.5)	290.6	(4.0)	290.5	(3.9)
O 1s	528.6	(1.5)	–	–	529.3	(1.8)	529.5	(2.0)
	–	–	531.7	(46.8)	–	–	531.8	(17.7)
	532.0	(47.2)	–	–	532.1	(33.5)	–	–
	–	–	–	–	533.1	(5.7)	533.0	(11.0)
Li 1s	55.4	(28.1)	55.2	(24.1)	55.7	(30.7)	56.0	(19.0)
F 1s	–	–	684.8	(0.8)	685.6	(1.8)	685.4	(7.0)
	687.5	(0.3)	–	–	–	–	–	–
P 2p	N.D.		N.D.		N.D.		N.D.	
Sn 3d	N.D.		484.9	(0.01)	484.7	(0.01)	485.3	(0.02)
			486.8	(0.04)	486.0	(0.01)	486.5	(0.03)
			492.6	(0.01)	493.2	(0.01)	493.6	(0.01)
			494.3	(0.03)	494.5	(0.01)	494.7	(0.02)

N.D.: not detected.

2.2. XPS

XPS measurements were carried out with a Thermo Scientific K-Alpha X-ray photoelectron spectrometer, using a focused monochromatized AlKα radiation ($h\nu = 1486.6$ eV). The XPS spectrometer was directly connected through a glove box under argon atmosphere, in order to avoid moisture/air exposure of the samples. For the Ag 3d5/2 line the full width at half-maximum (FWHM) was 0.50 eV under the recording conditions. The X-ray spot size was 400 μm. Peaks were recorded with constant pass energy of 20 eV. The pressure in the analysis chamber was less than 2×10^{-7} Pa. Short acquisition time spectra were recorded at the beginning and at the end of each experiment to check that the samples did not suffer from degradation during the measurements. The binding energy scale was calibrated from the hydrocarbon contamination using the C 1s peak at 285.0 eV. Core peaks were analyzed using a nonlinear Shirley-type background [33]. The peak positions and areas were optimized by a weighted least-squares fitting method using 70% Gaussian, 30% Lorentzian line shapes. Quantification was performed on the basis of Scofield's relative sensitivity factors. [34] TiSnSb electrodes were thoroughly rinsed with pure DMC and dried before XPS measurements, it is assumed that there was no trace of $LiPF_6$ salt and solvents left at the electrode surface during these measurements. For each electrode sample, several XPS analyses were performed at different positions to make the results statistically reliable.

2.3. SEM

The morphology and the texture of the electrodes were examined by a scanning electron microscope (JEOL 7600).

3. Electrochemical properties of TiSnSb electrode

CV was performed to highlight the irreversible processes occurring during the first reduction before the conversion reaction. Results presented in Fig. 1 (the inset is an enlargement of the SEI formation region) show the electrochemical reactions which occur in the electrolyte in the 0.5–2 V potential range. In this range, three reduction processes are identified. The small peaks at 0.78 V and 0.66 V can be assigned to the reduction of Sn, Ti and Sb oxides, such as SnO_2, TiO_2, Sb_2O_3 or Sb_2O_4, at the electrode surface [17]. These peaks are always visible even when the electrolyte formulation is changed (Fig. 1a and b). The first peak located at 1.15 V (Fig. 1a) could be assigned to the irreversible reduction of vinylene carbonate (VC) and formation of alkylcarbonate and polycarbonate species on the electrode surface. Further reduction of cyclic carbonates, EC and PC, is expected to occur at lower potential, below 0.7 V [35]. Fig. 1b shows the first CV cycle after addition of FEC to the electrolyte. From the inset in Fig. 1b one can see that the first reduction peak is shifted to a higher potential. This means that a more efficient SEI layer is expected to grow since it is formed at a higher potential than without FEC, and thus preventing further

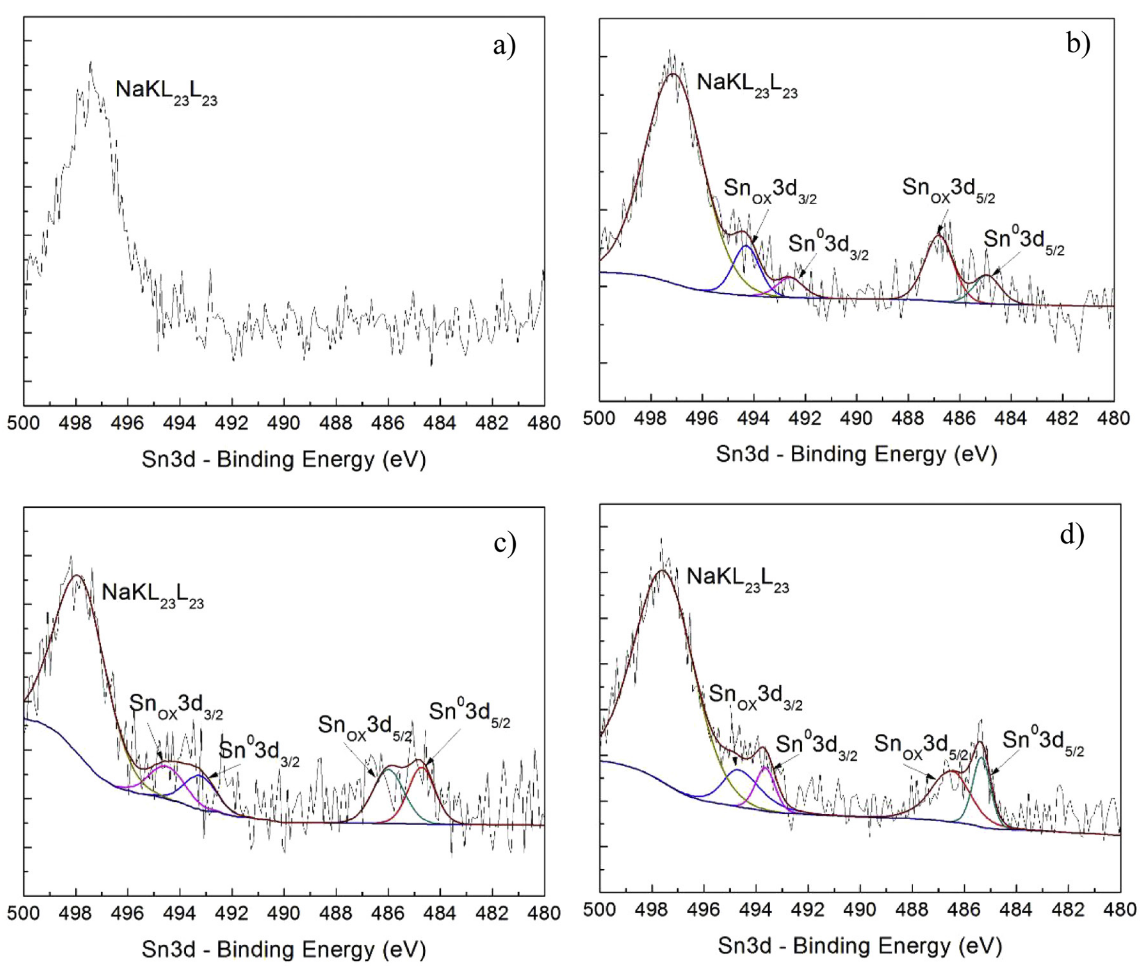

Fig. 4. XPS Sn 3d core peak spectra recorded at a) the end of 1st discharge without FEC, b) the end of 1st charge without FEC, c) the end of 1st discharge with FEC, d) the end of 1st charge with FEC.

electrolyte decomposition. Furthermore, the conversion peak, observed at 0.125 V is thinner and more intense when FEC is used. So we can expect from theses observations that the conversion reaction is faster when FEC is used as an additional additive to the electrolyte.

TiSnSb electrode undergoes a low voltage discharge and a large irreversible capacity during the 1st cycle, as shown in Fig. 2.

The discharge profile indicates the global shape of the galvanostatic curves are the same, which reveals that the electrochemical processes are unmodified by the additive: a rapid decrease of the potential down to a plateau at 0.5 V and then to a second plateau at 0.25 V. The lengths of these plateaus correspond respectively to the lithiation of Sb and Sn. In Fig. 2a, the galvanostatic curves indicate that the reduction of the standard electrolyte solution is equivalent to the insertion of 6.9 Li per formula unit, which is more than the 6.5Li corresponding to Li_3Sb and Li_7Sn_2 phases' formation. When FEC is added to the electrolyte, 5.5Li per formula unit are inserted in the active material as shown in Fig. 2b. During the reverse scan, 5.1Li and 4.3Li per formula unit can be removed from the active material respectively in the absence and the presence of FEC. As a conclusion, the addition of FEC induces both a reduction of the irreversible capacity (from 1.8Li to 1.2Li) and of the reversible capacity at the first cycle (5.1Li to 4.3Li) which correspond to 26 and 22% of irreversibility respectively. As FEC is reduced before VC and others electrolyte components, the SEI composition must contain more reduction products coming from FEC than VC and the smaller irreversible capacity indicates that FEC is an efficient SEI former additive.

Galvanostatic curves obtained at the 20th cycle exhibit similar shape to that at the first cycle as shown in Fig. 3a and Fig. 3b. Measurements of the capacity retention during the first 20 cycles of TiSnSb electrode in the standard electrolyte (containing VC) with or without FEC are displayed in Fig. 3c and Fig. 3d. The irreversible capacity becomes negligible for both electrolytes after five cycles which means that the coulombic efficiency approaches 100% during the following cycles. Nevertheless, the cell using the FEC-containing electrolyte displays better cycling performances as the specific capacity is maintained steady at 450 mAh g^{-1} from the second to the 20th cycle, while it is continuously fading down to 415 mAh g^{-1} at the 20th cycle in the absence of FEC. This is another proof that FEC helps to form a more stable SEI layer at the electrode surface.

4. Surface analysis results

4.1. XPS results

4.1.1. 1st Cycle

Table 1 displays XPS quantification data of 1s peaks for C, O, Li, F and 3d core peaks for Sn. Although titanium and antimony are reoxidized upon charge, XPS analysis at electrode surface revealed that these two species are not observed after cycling. Concerning

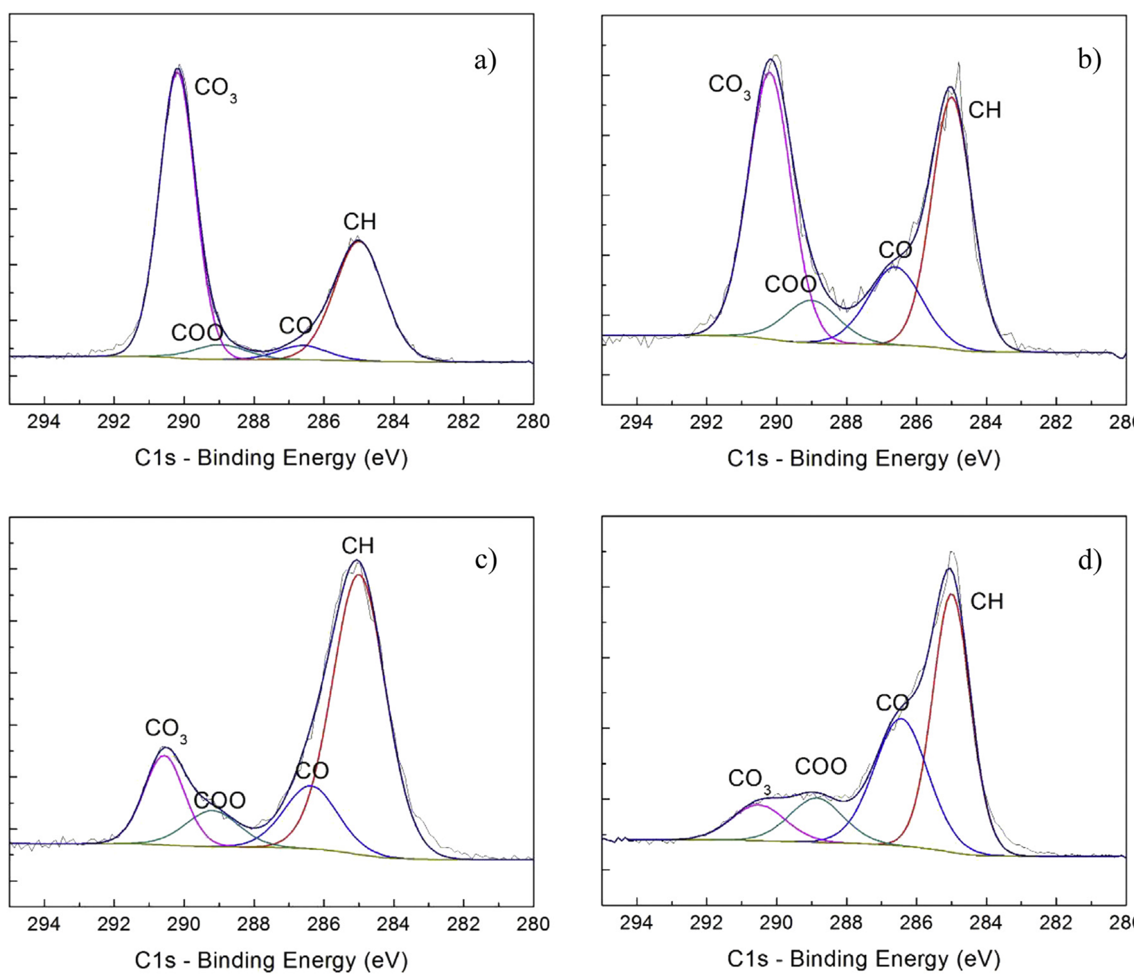

Fig. 5. XPS C 1s core peak spectra recorded at a) the end of 1st discharge without FEC, b) the end of 1st charge without FEC, c) the end of 1st discharge with FEC, d) the end of 1st charge with FEC.

the absence of Ti species, it is assumed that the lithiated Li_7Sn_2 and Li_3Sb phases, formed upon Li insertion at the surface of the material particle, dissimulate Ti buried in the bulk. The signal of Sn and Sb species are hence more easily detected than the non-electrochemically active Ti within the analysis depth of XPS. This assumption is supported by the detection of Ti species in Ti 2p core peak spectra (not given here) after mechanical removal (blade-scratching) of the top layer (<5 nm) of the electrode surface. On the other hand, Sb 3d core peak spectra share the same range of binding energies than that of oxygen, leading to an overlap of Sb and O peaks. From a quantitative point of view, the amount of Sb species at the surface is relatively low as compared with that of oxygen. Therefore, O 1s spectra will be considered containing only O species in the following discussion. As a result, Sn species are the only really distinguishable component of the active material.

The XPS Sn 3d core peak spectra recorded at the end of the first discharge and first charge are presented in Fig. 4. Binding energies of 484.7 eV and 493.2 eV are assigned to metallic tin and binding energies of 486.0 eV and 494.5 eV are assigned to tin oxide. The corresponding quantification data are presented in Table 1. In addition, the auger peak of sodium is also observed in the Sn 3d spectra at a binding energy around 498 eV. During XPS experiments, it is common to observe some Auger peaks, the nomenclature for which is based on the X-rays nomenclature. The designation of levels to the K, L, M, … shells is based on their having principal quantum numbers of 1, 2, 3, … respectively. Without FEC, there is no tin species detected in the analysis depth of XPS at the end of the first discharge. In the case of a charged electrode, Sn species could be detected (metallic Sn is 0.02%, Sn oxide is 0.07%). On the other hand, with the addition of FEC, a small amount of tin species can be observed both at the discharged and the charged state. It is worth noticing that the quantitative analysis indicates that the amount of Sn species is higher at the charged state than at the discharged state in both cases with or without the addition of FEC.

The XPS C 1s (Fig. 5) core peak spectra provide valuable information regarding the SEI nature when jointly analyzed with the O 1s (Fig. 6) and Li 1s core peaks. The F 1s and P 2p core peaks are displayed in Table 1 with the corresponding binding energies.

The component with a binding energy of 285.0 eV is assigned to CH_x environment, which is attributed to hydrocarbon contamination (always detected at the extreme surface) and to carbon atoms of organic species bound to carbon or hydrogen atoms only. The component observed at 286.5 eV can be assigned to carbon atoms bound to one oxygen atom (C—O), while the component at 289.0 eV corresponds to carbon atoms bound to two oxygen atoms (O═C—O). The component observed at 290.2 eV is the characteristic of carbon bound to three oxygen atom, which is typical of carbonate-like species ($-CO_3$) that could be Li_2CO_3 or lithium alkyl carbonates $ROCO_2Li$.

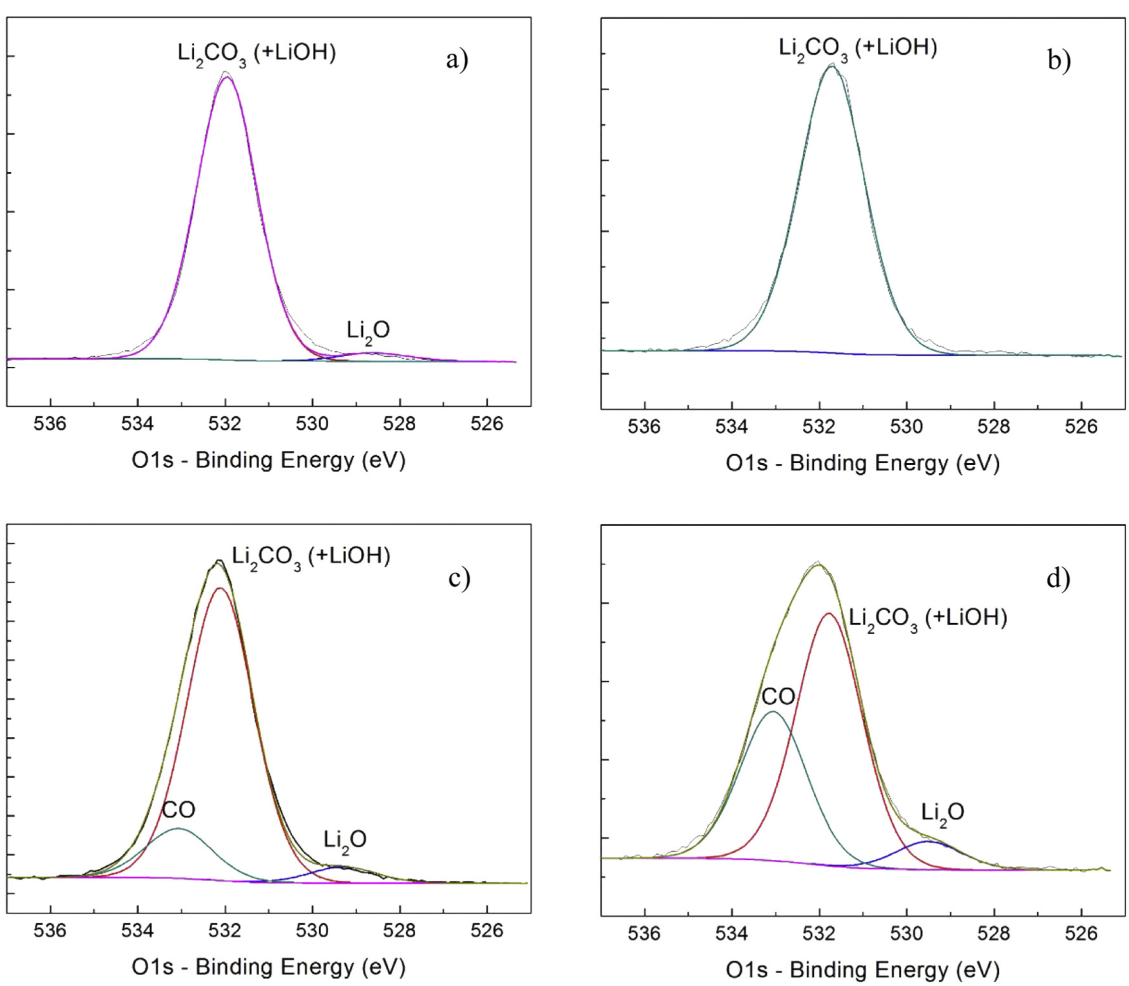

Fig. 6. XPS O 1s core peak spectra recorded at a) the end of 1st discharge without FEC, b) the end of 1st charge without FEC, c) the end of 1st discharge with FEC, d) the end of 1st charge with FEC.

Table 2
XPS quantification data recorded at the end of the 20th discharge without FEC (D20-4C), at the end of the 20th charge without FEC (C20-4C), at the end of the 20th discharge with FEC (D20-4C-FEC), and at the end of the 20th charge with FEC (C20-4C-FEC).

	D20-4C		C20-4C		D20-4C-FEC		C20-4C-FEC	
	B.E. (eV)	Atom (%)	B.E. (eV)	Atom (%)	B.E. (eV)	Atom (%)	B.E. (eV)	Atom (%)
C 1s	285.0	(23.1)	285.0	(29.2)	285.0	(16.1)	285.0	(24.0)
	286.5	(6.6)	286.6	(11.2)	286.7	(2.3)	286.6	(11.9)
	289.0	(1.4)	288.4	(2.4)	288.8	(1.6)	288.7	(4.0)
	290.4	(1.6)	290.6	(3.1)	290.2	(10.6)	290.5	(5.3)
O 1s	528.7	(5.6)	528.7	(1.4)	528.7	(1.8)	529.1	(1.0)
	531.5	(28.9)	531.5	(24.6)	531.9	(40.1)	531.5	(11.6)
	–	–	532.8	(4.8)	–	–	532.7	(17.4)
	–	–	534.0	(3.6)	–	–	534.3	(1.4)
Li 1s	55.4	(30.9)	55.8	(17.7)	55.5	(26.9)	56.0	(18.0)
F 1s	685.4	(1.2)	684.9	(1.3)	685.0	(0.5)	685.5	(3.9)
	687.6	(0.3)	687.1	(0.9)	686.9	(0.1)	687.9	(0.3)
P 2p	133.5	(0.3)	134.0	(0.5)	N.D.		133.8	(0.7)
	136.9	(0.1)	136.6	(0.1)			–	–
Sn 3d	N.D.		N.D.		N.D.		484.9	(0.01)
							486.8	(0.02)
							492.7	(0.01)
							494.2	(0.01)

N.D.: not detected.

The detailed quantification data are given in Table 1. In the presence of FEC, the amount of CO_3-like carbon decreases from 13.4% to 4.0% at the end of discharge, and from 11.5% to 3.9% at the end of charge. Charged electrodes exhibit less CO_3 compounds in both cases with or without FEC. The amount of C–O compounds increases with the presence of FEC from 0.9% to 3.7% at the discharged state, and from 4.2% to 13.8% at the charged state.

Without FEC, the O 1s core peak spectra (Fig. 6) at the end of discharge or charge present a broad peak, located around 531.8 eV which could be attributed either to Li_2CO_3 (532.2 eV) and/or LiOH (531.5 eV). Note that the small intensity component detected at the end of discharge, at 528.7 eV, is assigned to Li_2O. With FEC, the broad peak (33.5% of all the detected atoms) observed in the discharged electrode is located at a binding energy of 532.1 eV. The amount of Li_2O is 1.8%, quite similar to 1.5% in the electrode without FEC. On the other hand, in the charged electrode, Li_2CO_3 is still the major compound around 17.7%, although much lower than that of the electrodes cycled without FEC. Note that the total amount of O species decreased from 41.0% to 30.8% after the charge process. The amount of Li_2O is 2.0% compared to 0% in the electrode cycled without FEC. The peak located at 533.0 eV (5.7% and 11.0% respectively at the end of the discharge and charge) can be assigned to a CO environment, and will be assigned in the following discussion.

The Li 1s core peak spectra (55.2 eV) present the Li_2CO_3 and LiOH components when the TiSnSb electrode was cycled without FEC. The total amounts of Li species are 28.1% and 24.1% for

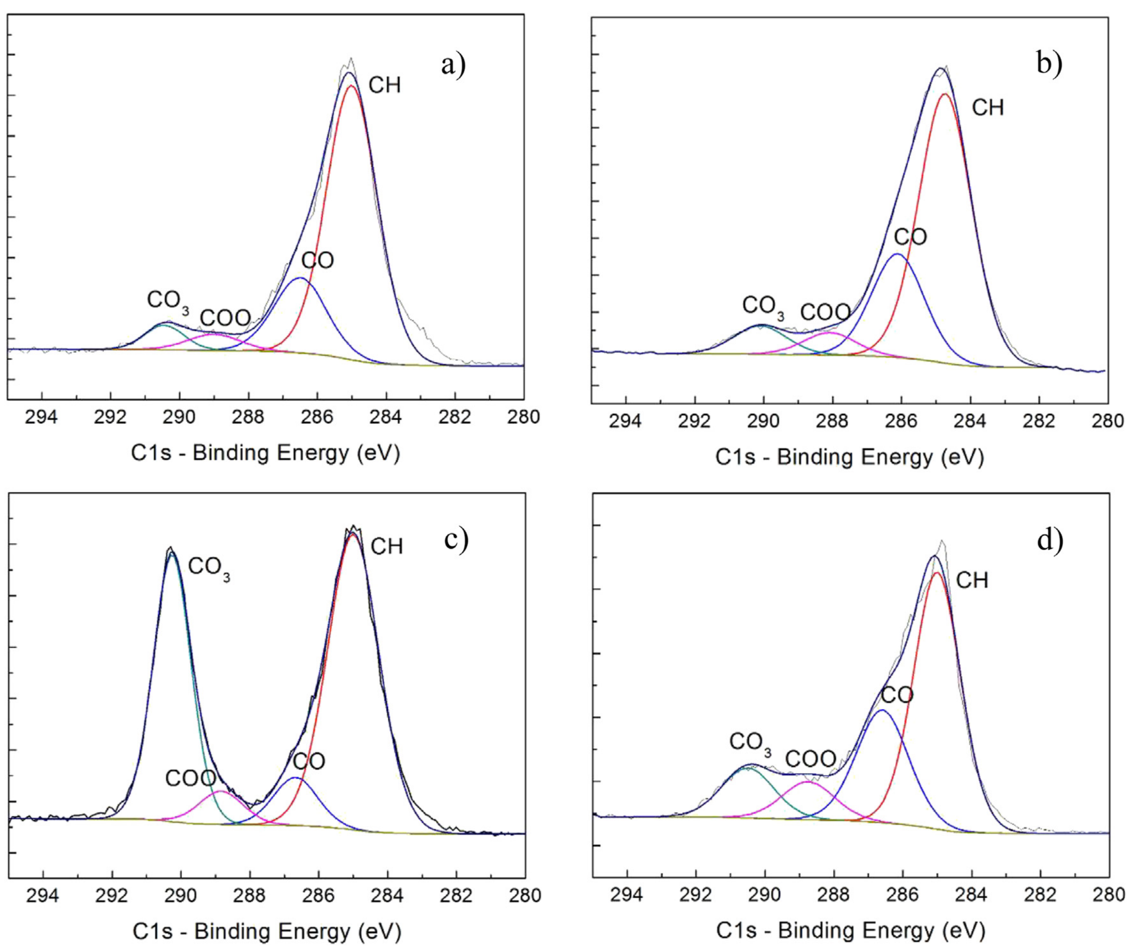

Fig. 7. XPS C 1s core peak spectra recorded at a) the end of 20th discharge without FEC, b) the end of 20th charge without FEC, c) the end of 20th discharge with FEC, d) the end of 20th charge with FEC.

discharged and charged electrodes respectively. With FEC, the Li 1s core peaks are located at binding energies of 55.7 eV and 56.0 eV for discharged and charged electrodes. The total amount of Li species decreased from 30.7% in the discharged electrode to 19.0% in the charged electrode.

The F 1s core peak (Table 1) are characterized by a main component at 685.0 eV, which could be assigned to LiF, and by a very weak component at 687.5 eV attributed to $LiPF_6$ (only observed for discharge electrode without FEC). In the presence of FEC, the amount of LiF increases from 1.8% (discharge state) to 7.0% at the end of charge. In general, charged electrodes exhibit a higher amount of LiF at their surface in both cases (i.e. with or without FEC).

4.1.2. 20th Cycle

Table 2 displays XPS quantification data of C 1s, O 1s, Li 1s, F 1s and Sn 3d core peaks. As for the first cycle, the elements present in the active material are difficult to observe. Only Sn species (metallic Sn of 0.02%, Sn oxide of 0.03%) are observed at the charged state and in the presence of FEC.

The XPS C 1s core peak spectra recorded after the 20th discharge/charge is presented in Fig. 7. As in the 1st cycle, the components with binding energies of 285.0 eV, 286.5 eV, 289.0 eV, and 290.2 eV are attributed to CH_x, C–O, O=C–O, and $-CO_3$ species, respectively.

With the presence of FEC, the amount of $-CO_3$ increases from 1.6% to 10.6% at the end of discharge, from 3.1% to 5.3% at the end of charge according to the quantification data given in Table 2.

Without FEC, at the end of the discharge, the broad peak observed in the XPS O 1s core peak spectra (Fig. 8) located at 531.5 eV could be mainly attributed to LiOH as the major component. The peak located at low binding energy (528.7 eV) is assigned to Li_2O (5.6%). In the charged electrode, the O1s peak is composed of multiple components located at 528.7, 531.5, 532.8 and 534.0 eV attributed respectively to Li_2O, LiOH, C–O and POF_x environments.

With FEC, in the discharged electrode, the broad peak located at 531.9 eV represents Li_2CO_3 as the major component (40.1%). This result is in agreement with the corresponding C 1s spectrum, where CO_3 is 10.6% with FEC (and 1.6% without FEC). The amount of Li_2O is 1.8%, lower than that of 5.6% in the electrode cycled without FEC.

In the charged electrode, the broad peak is composed of multiple components: LiOH (11.6%), CO environment (532.7, 17.4%) and probably POF_x (534.3 eV, 1.4%). The amount of Li_2O (529.1 eV) is 1.0% compared to 1.4% in the electrode without FEC. The total amount of O species decreases from 41.9% to 31.4% after charge process as already observed during 1st cycle with presence of FEC (from 41.0% to 30.8%).

A small amount of LiF (F 1s: 685 eV) is detected. In the presence of FEC, it increases from 0.5% to 3.9% between discharged and charged states. Note also that a few amount of $LiPF_6$ salt is observed

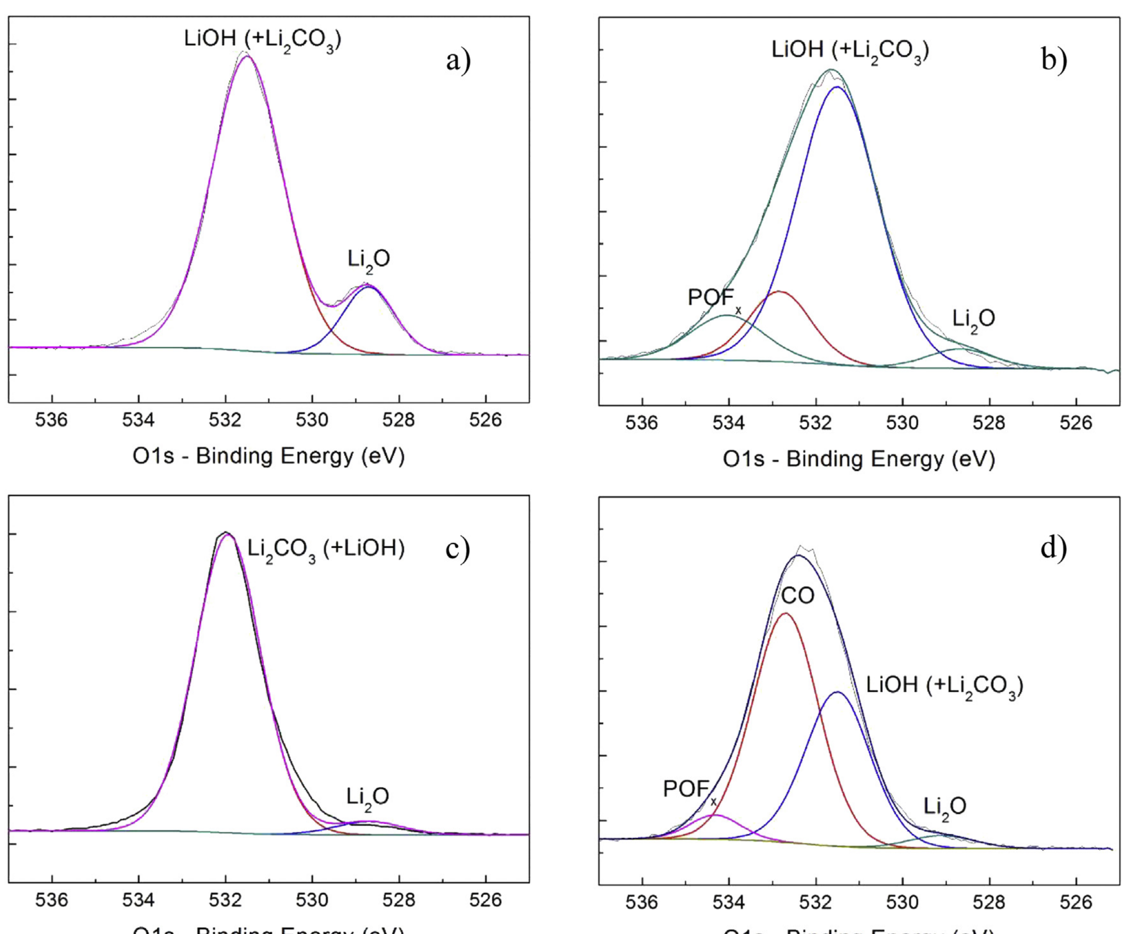

Fig. 8. XPS O 1s core peak spectra recorded at a) the end of 20th discharge without FEC, b) the end of 20th charge without FEC, c) the end of 20th discharge with FEC, d) the end of 20th charge with FEC.

for all electrodes analyzed at the 20th cycle. In general, charged electrodes bear a higher total amount of F species with or without FEC.

4.2. EIS results

In order to evaluate the effect of FEC, comparisons based on different element in EIS spectra during the 1st cycle are displayed in Fig. 9. In Fig. 9a, EIS spectra are collected at the end of 1st charge at 1.6 V, where in the HF domain (9867 Hz) the resistance of interfaces, which includes SEI layer, is lower in FEC-containing. EIS spectra recorded at 0.5 V are presented in Fig. 9b, where the depressed shape of the semi-circle indicates the contribution from both interface resistance and charge transfer, and at lower frequencies, the straight line at 45° is assigned to Warburg element that represents Li diffusion through the TiSnSb electrode. It is worth to notice that the resistance attributed to charge transfer in the MF domain at 142 Hz drastically decreases from 60 Ω to 20 Ω with the addition of FEC in the electrolyte. Then at the end of the 1st discharge (0.02 V) as shown in Fig. 9c, an inductive loop in the LF range is clearly observed in the electrode using standard electrolyte, while with the addition of FEC the inductive loop almost disappears. Furthermore, the interfaces and charge transfer resistances decreases. In addition, the inductive loop is less important at low cycling rates (C) than high cycling rates (4 C) as indicated by the EIS reported in Fig. 9d.

4.3. SEM analysis

The surface morphology of pristine TiSnSb electrode is presented in Fig. 10. SEM images illustrate that TiSnSb micro-particles are evenly distributed at the electrode surface (Fig. 10a) and in the bulk material based on the cross-section view (Fig. 10b). Under a higher magnification, in agreement with the high porosity of the electrode (60%) displays a texture that is favorable to material volume change during lithiation as the net formed by VGCF fibers where the TiSnSb micro-particles get entangled is also tightened by the CMC binder (Fig. 10c). The corresponding backscattered electron (BSE) image (Fig. 10d) indicates that the TiSnSb micro-particles (bright area) and carbon fibers (dark area) are clearly distinguishable.

The surface morphology of TiSnSb electrode cycled after the 20th discharge is presented in Fig. 11a, where carbon fibers and the TiSnSb micro-particles are clearly covered by a surface layer. At the end of 20th charge this surface layer disappears (Fig. 11b).

5. Discussions

5.1. 1st Cycle

Firstly, the discussion will be focused on the thickness of the SEI layer during the 1st cycle. Without the addition of FEC, no tin species is detected in the analysis depth of XPS (5 nm) at the end of discharge, which illustrates that SEI layer is at least thicker than 5 nm. However, Sn species are detectable from the electrode at the charged state, around 0.1%. Since signals of Sn are given by the active material that is covered by SEI, this means SEI layer is thinner at the charged state. From the end of discharge to the end of charge, XPS analysis suggests that the SEI layer partially dissolved during the charge process.

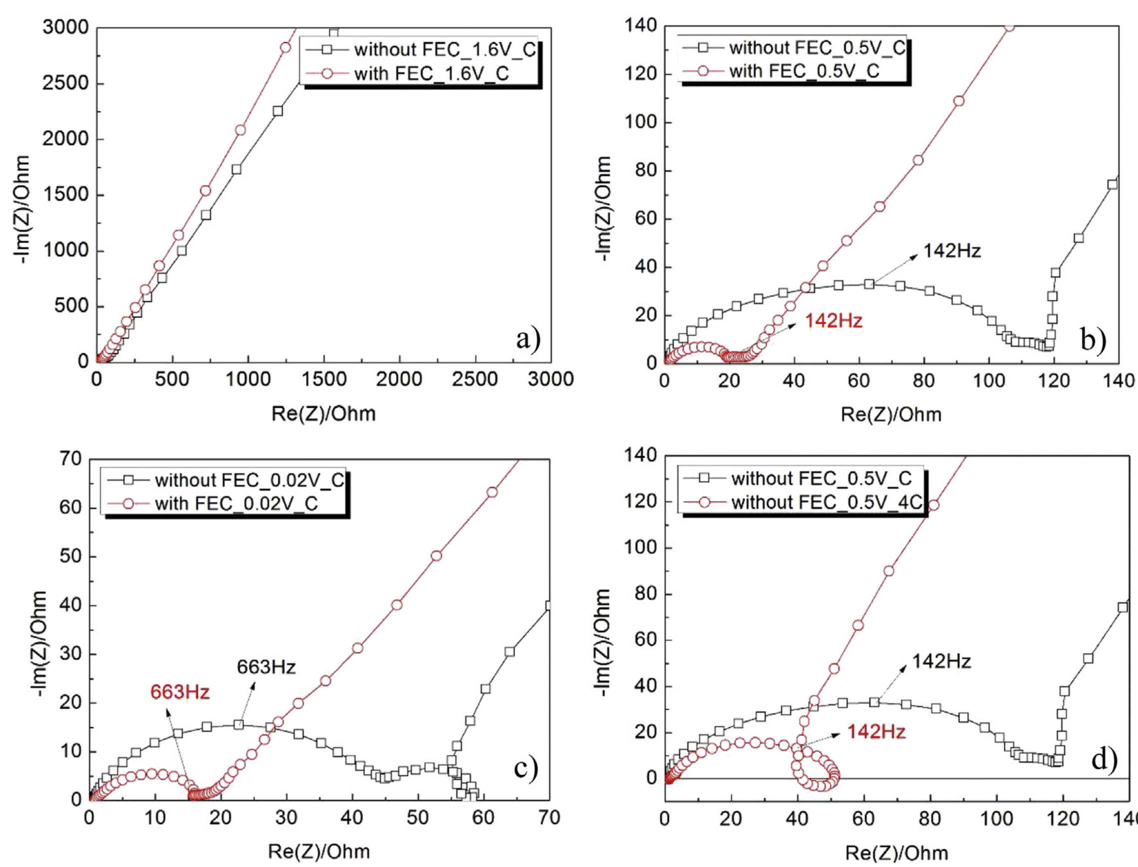

Fig. 9. EIS spectra recorded a) at the end of the 1st charge at 1.6 V, b) at 0.5 V, c) at the end of the 1st discharge at 0.02 V, d) at 0.5 V and cycling rates of 4 C and C.

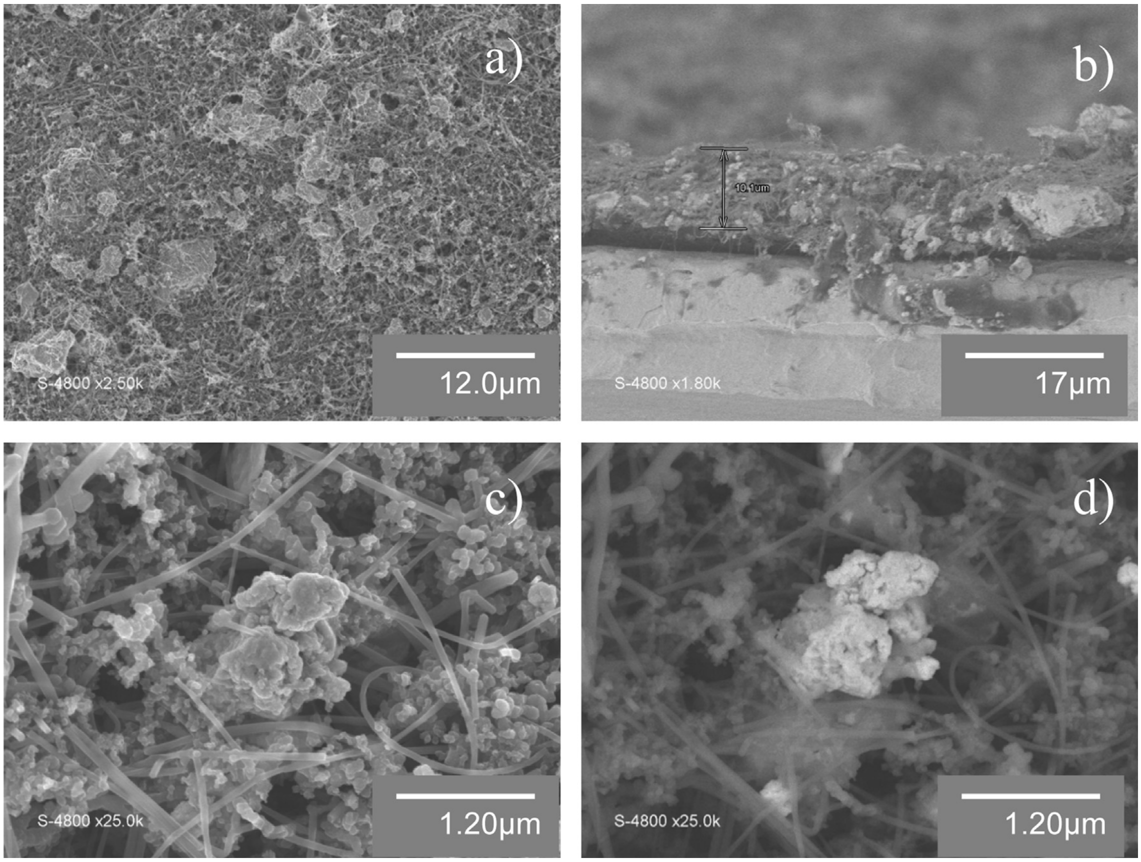

Fig. 10. SEM images of pristine TiSnSb electrode, a) top view in the scale of 12.0 μm, b) cross-section view in the scale of 17 μm, c) top view in the scale of 1.20 μm, d) BSE image of Fig. 10c.

With the addition of FEC, the Sn 3d spectrum of the discharged electrode presents a small amount of tin species, which indicates that the SEI thickness is close to the analysis depth. As Sn species are detectable in the electrode cycled with FEC, we may conclude that the presence of FEC results in a thinner SEI layer compared to those electrodes cycled with the standard electrolyte which contains only VC as additive. Conclusion of thinner SEI formed in FEC-containing electrolyte was also made in a previous work on SiNW electrodes [29]. Partial dissolution of the SEI layer during the charge process occurs, in the presence or not of FEC. In addition, the presence of LiF in the electrode cycled with FEC may further prove a thinner SEI layer as well.

EIS results demonstrates that when FEC is added, the HF and MF semi-circle decreases in size, which indicates lower interface and charge transfer resistances. This correlates well with the presence of a thinner SEI layer as indicated by XPS analysis.

In addition, the inductive loop recorded in the EIS spectra is not observed in the HF but only in the LF range, which has also been reported in other studies [36,37]. This phenomenon usually exists under the conditions of rough electrodes or electrosorption of corrosion process [38,39] fuel cells [40] and electrodeposition systems [41]. J. Song et al. [42] suggest that this inductive loop corresponds to adsorption of lithium ions on carbon surface during lithium intercalation into carbon. Thus the appearance of inductive loop could be only due to properties of SEI layer which is modified by the electrolyte additives or the cycling rate but not to some artificial effects. Having accepted this premise, we propose that the formation of an inductive loop could be attributed to the adsorption of ions in a porous, thick and imperfect SEI.

Another possible mechanism leading to such an inductive loop could be a current flow occurring between particles having different state of charge [43], illustrated by the scheme reported in Fig. 12. When lithium ions are inserted into TiSnSb electrode during discharge, lithium rich and lithium deficient regions in the electrode may be isolated by the SEI film (due to imbalanced electronic continuity). In this case a concentration cell is built between a fully and a partially lithiated antimony or tin alloy and the current flows within this concentration cell is opposite to the direction of lithium insertion. Such situation accomplishes the requirements to form an inductive loop.

As inductive loops become smaller in size when FEC is added, this could contribute to show that the quality of the SEI is improved by the FEC additive, and indicate a more homogeneous SEI layer no matter which mechanism leading to the inductive loop is operating. In addition, as shown in Fig. 9d, the magnitude of the inductive loop depends on the cycling rate. The inductive loop is larger when the electrode is cycled at a relatively high regime of 4 C, and it almost disappears when the cycling rate is decreased to 1 C. This is in agreement with the schematic presentation of Fig. 12 where high cycling rates could then promote the formation of alloys with different state of charge (lithiation). Indeed, lithiation is more favorable at lower cycling rate even if it is improved by the addition of FEC.

Secondly, the evolution of the chemical nature of the SEI layer will be discussed. Without FEC, the presence of Li_2CO_3 in C 1s core peak spectra results in a peak at 290.2 eV corresponding to $-CO_3$ species, while $ROCO_2Li$ species presents two peaks of equal intensity at 290.2 eV and 286.5 eV due to the same number of carbon atoms present in CO and CO_3 environment. Since the C 1s core peak spectra displayed in Fig. 3 does not support the presence of

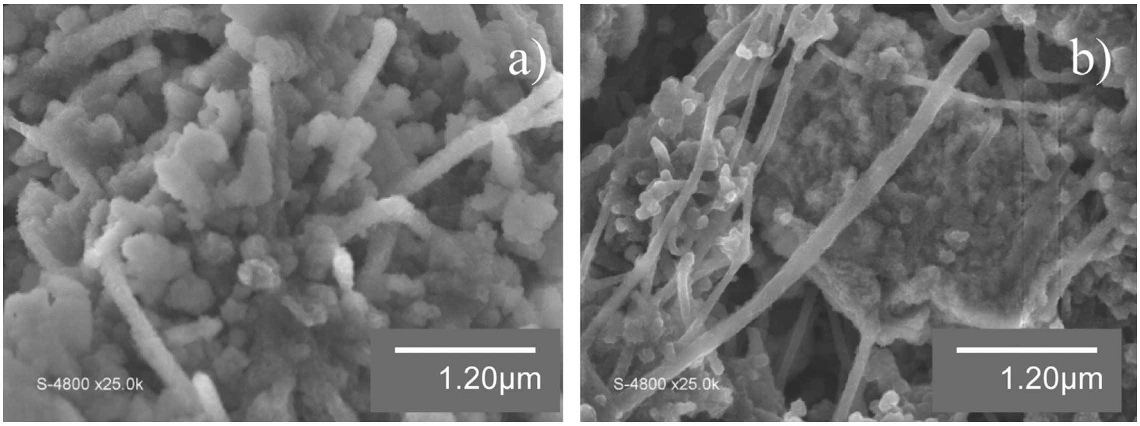

Fig. 11. SEM images on the same scale of TiSnSb electrodes cycled with FEC, a) at the end of 20th discharge, b) at the end of 20th charge.

$ROCO_2Li$, Li_2CO_3 could be considered as the major component among these two species. Moreover, from a quantitative point of view, the relative proportion of C to O in Li_2CO_3 equals to 1:3 and the excess amount of the species in the corresponding O 1s spectra may indicate the formation of LiOH (531.5 eV). The origin of LiOH can be assigned to water contamination, which comes from CMC binder present in the electrode formulation. It is worth noticing that the decomposition of LiOH phase into Li_2O and H_2O under the X-ray beam in ultra-high vacuum has often been observed. Therefore, Li_2CO_3 is the major component accompany with LiOH at the extreme surface of the SEI layer in the absence of FEC.

On the other hand with the presence of FEC, the increase in C–O and the decrease in CO_3 species observed in the C 1s quantification data indicate that there may be a composition change at the extreme surface of the SEI layer. Especially at the end of discharge, where data indicate a relative proportion for these two components equal to 3.7:4.0, which suggests that $ROCO_2Li$ instead of Li_2CO_3 is now the major carbonate species. In the corresponding O 1s spectrum, the broad peak observed at a binding energy of 532.1 eV can be assigned to a mixture of oxygen atoms presented in the environment of Li_2CO_3 (532.2 eV), LiOH and also the C–O (533.0 eV) which can be also assigned to $ROCO_2Li$. At the charged state, in spite of $ROCO_2Li$ that presents C–O environment, the excess amount of CO species given in the quantification data of C 1s may be assigned to other degradation products like ROLi or PEO oligomers $(-CH_2-CH_2-O-)_n$ [44], for which carbon atoms are in a one-oxygen environment. The presence of LiF (55.9 eV) is confirmed by its corresponding quantification data presented in Table 1 (1.8% for discharged electrode, 7.0% for charged electrode), and in the Li 1s spectra of the discharged electrode, the broad peak is also attributed to: Li_2CO_3, LiOH, $ROCO_2Li$ and LiF. Therefore, $ROCO_2Li$ and LiF together with LiOH are the major components in the presence of FEC.

Hence, Li_2CO_3 is suggested as the major component of the SEI layer when using standard electrolyte, while $ROCO_2Li$ and LiF are detected when using FEC-containing electrolyte. This result reveals that the addition of FEC modifies the chemical composition of the very near surface (~5 nm) of the SEI layer.

5.2. The 20th cycle

As indicated in the discussion of the 1st cycle, after the partial dissolution during charge process, there is 0.1% Sn species in total observed at the end of 1st charge. However, after 20 cycles without the addition of FEC, none of the Sn 3d spectra indicate Sn species at their extreme surface, which demonstrates that SEI layer grows thicker than the analysis depth of XPS (5 nm) upon cycling.

With the addition of FEC, Sn species are present at 20th discharge and this amount has to be compared to the 0.04% Sn species detected at the end of the 1st discharge. This leads to the conclusion that we made for the electrodes cycled without FEC: SEI layer grows thicker than the analysis depth of XPS upon cycling. Nevertheless, at the charged state, the presence of Sn species implies that the SEI thickness is again close to the analysis depth after the partial dissolution during the charge process. This confirms that

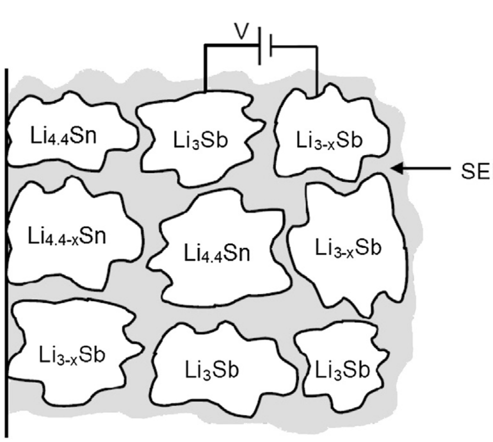

Fig. 12. Schematic presentation of the mechanism where a current flow occurs between particles having different state of charge.

Table 3
Summary of the XPS quantification data in Tables 1 and 2. At the end of the 1st discharge without FEC (D1-4C)/with FEC (D1-4C-FEC), at the end of the 1st charge without FEC (C1-4C)/with FEC (C1-4C-FEC), at the end of the 20th discharge without FEC (D20-4C)/with FEC (D20-4C-FEC), and at the end of the 20th charge without FEC (C20-4C)/with FEC (C20-4C-FEC).

	C 1s	O 1s		Li 1s	F 1s
	CO_3	Li_2O	Broad peak	Total	LiF
	Atom (%)	Atom (%)	Atom (%)	Atom (%)	Atom (%)
D1-4C	(13.4)	(1.5)	(47.2)	(28.1)	–
C1-4C	(1.6)	(5.6)	(28.9)	(30.9)	(1.2)
D1-4C-FEC	(4.0)	(1.8)	(33.5)	(30.7)	(1.8)
C1-4C-FEC	(3.9)	(2.0)	(17.7)	(19.0)	(7.0)
D20-4C	(1.6)	(5.6)	(28.9)	(30.9)	(1.2)
C20-4C	(3.1)	(1.4)	(24.6)	(17.7)	(1.3)
D20-4C-FEC	(10.6)	(1.8)	(40.1)	(26.9)	(0.5)
C20-4C-FEC	(5.3)	(1.0)	(17.4)	(18.0)	(3.9)

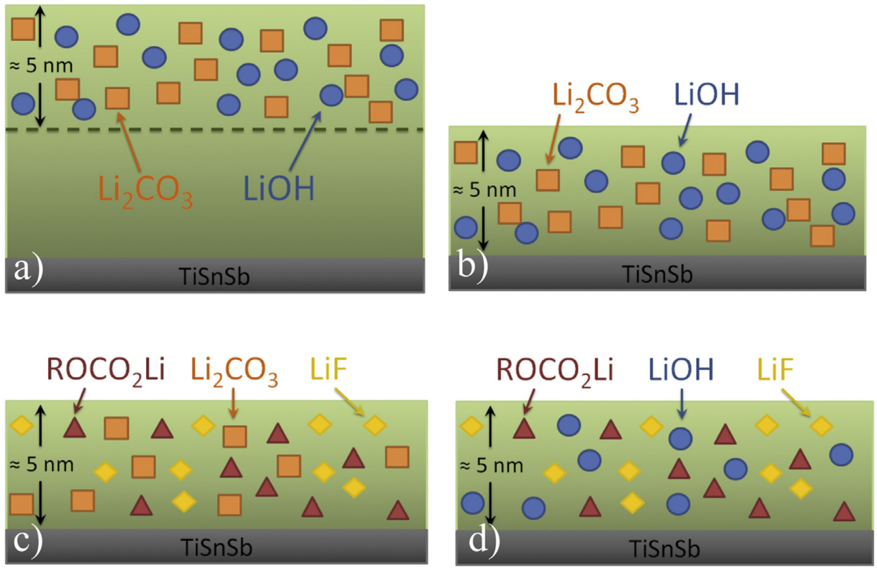

Fig. 13. Schematic diagram of the SEI layer formed at a) the end of 1st discharge without FEC, b) the end of 1st charge without FEC, c) the end of 1st discharge with FEC, d) the end of 1st charge with FEC.

the addition of FEC results in a thinner SEI for the 1st cycle as well as the 20th cycle.

Table 3 indicates also a significant decrease of CO_3 species from the 1st discharge (13.4%) to the 20th discharge (1.6%) when FEC is not added. Meanwhile in O 1s spectra, no CO environment related to $ROCO_2Li$ but instead a broad peak (28.9%) is observed at a binding energy of 531.5 eV, which can be mainly assigned to LiOH. Thus, at the end of the 20th discharge, the major component at the outermost surface of the SEI layer is no longer $-CO_3$ species but LiOH, which could still be attributed to the water contained in the CMC binder. As LiOH undergoes a transformation to Li_2O when it is exposed to X-ray beam, this may also explain a rather high amount of Li_2O (5.6%) detected in the O 1s spectra. At the charged state, although the amount of CO_3 species in C 1s spectrum is a little higher (3.1%) than that of the discharged state, the broad peak in the corresponding O 1s spectrum again indicates the mixture of Li_2CO_3 and LiOH, where LiOH is still the major component. As a result, LiOH together with Li_2CO_3 are the main species present at the surface of the electrode when using electrolyte without FEC.

On the other hand, in the presence of FEC, the amount of CO_3 in C 1s increases from the 1st discharge (4.0%) to the 20th discharge (10.6%). The broad peak (40.1%) in O 1s spectrum gives no evidence of CO environment associated to $ROCO_2Li$ but confirms $-CO_3$ species, which makes Li_2CO_3 the major carbonate-related species at the surface. In addition, the broad peak (26.9%) found at 55.6 eV in Li 1s spectra implies a mixture of LiOH, Li_2CO_3 and LiF (~1.0%).

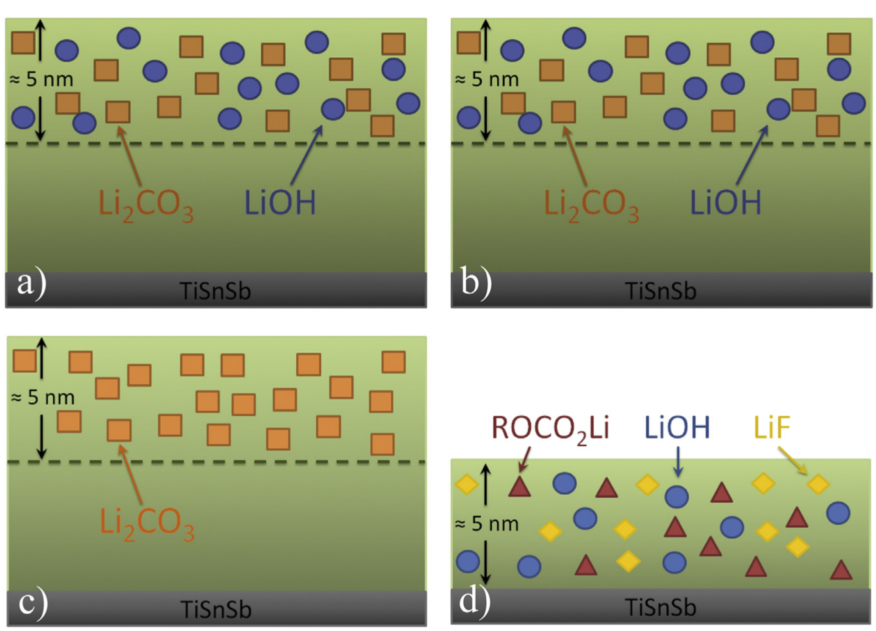

Fig. 14. Schematic diagram of the SEI layer formed at a) the end of 20th discharge without FEC, b) the end of 20th charge without FEC, c) the end of 20th discharge with FEC, d) the end of 20th charge with FEC.

At the charged state, the $-CO_3$ species detected in the C 1s spectrum together with the peak observed at 532.7 eV in O 1s spectrum, which can be assigned to CO environment in $ROCO_2Li$, suggesting the presence of $ROCO_2Li$ instead of Li_2CO_3. In addition, the existence of LiOH is confirmed by the detection of the 531.5 eV peak in O 1s spectrum. Furthermore, the quantification data of F 1s implies that LiF (3.9% in F 1s) could be considered as a major component at the surface. Thus, $ROCO_2Li$ and LiF accompanied with LiOH are suggested as the major components at the surface of the charged electrode with the addition of FEC.

There are a few more details to be noticed about LiF. The amount of LiF detected in the charged electrodes which is always higher than that of the discharged electrodes may support the hypothesis of a partial dissolution of SEI layer during the charge process, as degradation product from this salt should be the first layer deposited at the electrode surface. Moreover, the decreased amount of LiF after 20 cycles compared to that of the 1st cycle supports the idea that a growth of the SEI layer occurs upon cycling as already concluded from the discussion of Sn 3d spectra.

Impedance spectra exhibiting smaller capacitive semi-circles indicate that the SEI layer and that the charge transfer have a lower resistance meaning that a thinner or/and more conductive SEI layer is formed. The presence of Sn species in the XPS spectra indicate that the thickness reduction of the SEI is, at least partially due to the dissolution process which occurs when FEC is added. Moreover SEM images show that, in the presence of FEC, a homogeneous SEI layer (composed mainly Li_2CO_3) is observed at the 20th cycle which helps to explain the differences in nature of its outermost surface (Fig. 11). Figs. 13 and 14 summarize the main components present in the SEI as a function of the cycle number, the state of charge and the nature of the additives in the electrolyte. Components in the region deeper than 5 nm are not indicated in Figs. 13 and 14 due to experimental limitations. As a conclusion, using FEC as an electrolyte additive, which is able to enhance TiSnSb electrochemical properties, implies also significant modifications of the SEI layer composition and some of its components such as $ROCO_2Li$ and LiF may play an important role for that.

6. Conclusion

As suggested in previous works on Si-based electrodes, VC and FEC-containing electrolyte reduced the cumulative capacity losses as they favor the precipitation of more stable degradation products from the electrolyte and limit its further decomposition. XPS study confirmed that partial dissolution of SEI layer happens during cycling and that change in composition of its extreme surface occurs within the presence of FEC. Li_2CO_3, $ROCO_2Li$ and LiF SEI components may play an important role in the improvement of the cycling ability of the TiSnSb material. From EIS study, lower interfacial resistance and smaller inductive loops support the formation of a thinner and more conductive SEI layer which is also in accord with XPS analysis. EIS and XPS results are able to explain the enhanced electrochemical properties of TiSnSb electrode when FEC is added together with VC as additives in alkylcarbonate based electrolytes.

Acknowledgment

Financial support by the ANR (*Projet Blanc*) is gratefully acknowledged.

References

[1] P.G. Bruce, B. Scrosati, J.-M. Tarascon, Angew. Chem. Int. Ed. 47 (2008) 2980.
[2] O. Yamamoto, N. Imanishi, Y. Takeda, H. Kashiwagi, J. Power Sources 54 (1995) 72.
[3] L. Monconduit, J.C. Jumas, R. Alcántara, J.L. Tirado, C. Pérez Vicente, J. Power Sources 107 (2002) 74.
[4] L.M.L. Fransson, J.T. Vaughey, K. Edstrom, M.M. Thackeray, J. Electrochem. Soc. 150 (2003) A86.
[5] J. Xie, X. Zhao, G. Cao, Y. Zhong, M. Zhao, J. Electroanal. Chem. 542 (2003) 1.
[6] J. Xie, G. Cao, Y. Zhong, X.B. Zhao, J. Electroanal. Chem. 568 (2004) 323.
[7] R.J. Alcantara, F. Fernandez-Madrigal, P.L. Lavela, J. Tirado, J. Claude Jumas, J. Olivier-Fourcade, J. Mater. Chem. 9 (1999) 2517.
[8] J. Wolfenstine, S. Campos, D. Foster, J. Read, W.K. Behl, J. Power Sources 109 (2002) 230.
[9] Q.F. Dong, C.Z. Wu, M.G. Jin, Z.C. Huang, M.S. Zheng, J.K. You, Z.G. Lin, Solid State Ionics 167 (2004) 49.
[10] L. Fang, B.V.R. Chowdari, J. Power Sources 97–98 (2001) 181.
[11] K.K.D. Ehinon, S. Naille, R. Dedryvère, P.-E. Lippens, J.-C. Jumas, D. Gonbeau, Chem. Mater. 20 (2008) 5388.
[12] M.M. Thackeray, J.T. Vaughey, C.S. Johnson, A.J. Kropf, R. Benedek, L.M.L. Fransson, K. Edstrom, J. Power Sources 113 (2003) 124.
[13] X.Z. Liao, Z.F. Ma, H.H. Hu, Y.Z. Sun, X.X. Yuan, Electrochem. Commun. 5 (2003) 657.
[14] Martin Winter, Jürgen O. Besenhard, Electrochim. Acta 45 (1999) 31.
[15] M. Wachtler, J.O. Besenhard, M. Winter, J. Power Sources 94 (2001) 189.
[16] M.T. Sougrati, J. Fullenwarth, A. Debenedetti, B. Fraisse, J.C. Jumas, L. Monconduit, J. Mater. Chem. 21 (2011) 10069.
[17] C. Marino, A. Darwiche, N. Dupre, H.A. Wilhelm, B. Lestriez, H. Martinez, R. Dedryvere, W. Zhang, F. Ghamouss, D. Lemordant, L. Monconduit, J. Phys. Chem. C 117 (2013) 19302.
[18] E. Peled, J. Electrochem. Soc. 126 (1979) 2047.
[19] R. Fong, U. Von Sacken, J.R. Dahn, J. Electrochem. Soc. 137 (1990) 2009.
[20] D. Guyomard, J.-M. Tarascon, J. Electrochem. Soc. 140 (1993) 3071.
[21] Y. Ein-Eli, S.F. McDevitt, D. Aurbach, B. Markovsky, A. Schechter, J. Electrochem. Soc. 144 (1997) L180.
[22] J.O. Besenhard, M. Winter, J. Yang, W. Biberacher, J. Power Sources 54 (1995) 228.
[23] E. Peled, D. Golodnitsky, in: P.B. Balbuena, Y. Wang (Eds.), Lithium-Ion Batteries: Solid–Electrolyte Interphase, Imperial College Press, London, 2004.
[24] L. El Ouatani, R. Dedryvère, C. Siret, P. Biensan, S. Reynaud, P. Iratçabal, D. Gonbeau, J. Electrochem. Soc. 156 (2009) A103.
[25] M. Ulldemolins, F. Le Cras, B. Pecquenard, V.P. Phan, L. Martin, H. Martinez, J. Power Sources 206 (2012) 245.
[26] N.-S. Choi, Y. Lee, S. Kim, S.-C. Shin, Y.-M. Kang, J. Power Sources 195 (2010) 2368.
[27] L. Chen, K. Wang, X. Xie, J. Xie, J. Power Sources 174 (2007) 538.
[28] D. Mazouzi, N. Delpuech, Y. Oumellal, M. Gauthier, M. Cerbelaud, J. Gaubicher, N. Dupré, P. Moreau, D. Guyomard, L. Roué, B. Lestriez, J. Power Sources 220 (2012) 180.
[29] V. Etacheri, O. Haik, Y. Goffer, G.A. Roberts, I.C. Stefan, R. Fasching, D. Aurbach, Langmuir 28 (2012) 965.
[30] J. Qian, Y. Chen, L. Wu, Y. Cao, X. Ai, H. Yang, Chem. Commun. 48 (2012) 7070.
[31] S. Komaba, T. Ishikawa, N. Yabuuchi, W. Murata, A. Ito, Y. Ohsawa, ACS Appl. Mater. Interfaces 3 (2011) 4165.
[32] H.A. Wilhelm, C. Marino, A. Darwiche, L. Monconduit, B. Lestriez, Electrochem. Commun. 24 (2012) 89.
[33] D.A. Shirley, Phys. Rev. B 5 (1972) 4709.
[34] J.H. Scofield, J. Electron Spectrosc. Relat. Phenom. 8 (1976) 129.
[35] Xuerong Zhang, Robert Kostecki, Thomas J. Richardson, James K. Pugh, Pilip N. Ross Jr., J. Electrochem. Soc. 148 (2001) A1341.
[36] E. Karden, S. Buller, R.W. De Doncker, J. Power Sources 85 (2000) 72.
[37] G. Nagasubramanian, J. Power Sources 87 (2000) 226.
[38] N.A. Hampson, S.A.G.R. Karunathilaka, R. Leek, J. Appl. Electrochem. 10 (1980) 3.
[39] D.A. Harrington, B.E. Conway, Electrochim. Acta 32 (1987) 1703.
[40] J.T. Muller, P.M. Urban, W.F. Holderich, J. Power Sources 84 (1999) 157.
[41] R. Wiart, Electrochim. Acta 35 (1990) 1587.
[42] J.Y. Song, H.H. Lee, Y.Y. Wang, C.C. Wan, J. Power Sources 111 (2002) 255.
[43] Quan-Chao Zhuang, Xiang-Yun Qiu, Shou-Dong Xu, Ying-Huai Qiang, Shi-Gang Sun, Diagnosis of Electrochemical Impedance Spectroscopy in Lithium-Ion Batteries, in: Ilias Belharouak (Ed.), Lithium Ion Batteries – New Developments, InTech, 2012, ISBN 978-953-51-0077-5.
[44] R. Dedryvère, H. Martinez, S. Leroy, D. Lemordant, F. Bonhomme, P. Biensan, D. Gonbeau, J. Power Sources 174 (2007) 462.